Establishment of Patient-Derived Succinate Dehydrogenase–Deficient Gastrointestinal Stromal Tumor Models for Predicting Therapeutic Response

Mayra Yebra[1,2], Shruti Bhargava[1,2], Avi Kumar[1,3], Adam M. Burgoyne[1,4], Chih-Min Tang[1,2], Hyunho Yoon[1,2], Sudeep Banerjee[1,2], Joseph Aguilera[1,5], Thekla Cordes[1,3], Vipul Sheth[6], Sangkyu Noh[1,2], Rowan Ustoy[1,2], Sam Li[1,2], Sunil J. Advani[1,5], Christopher L. Corless[7], Michael C. Heinrich[8], Razelle Kurzrock[1,4,9], Scott M. Lippman[1,4,9], Paul T. Fanta[1,4,9], Olivier Harismendy[1,10], Christian Metallo[1,3,11,12], and Jason K. Sicklick[1,2,9]

ABSTRACT

Purpose: Gastrointestinal stromal tumor (GIST) is the most common sarcoma of the gastrointestinal tract, with mutant succinate dehydrogenase (*SDH*) subunits (A–D) comprising less than 7.5% (i.e., 150–200/year) of new cases annually in the United States. Contrary to GISTs harboring *KIT* or *PDGFRA* mutations, *SDH*-mutant GISTs affect adolescents/young adults, often metastasize, and are frequently resistant to tyrosine kinase inhibitors (TKI). Lack of human models for any *SDH*-mutant tumors, including GIST, has limited molecular characterization and drug discovery.

Experimental Design: We describe methods for establishing novel patient-derived *SDH*-mutant (m*SDH*) GIST models and interrogated the efficacy of temozolomide on these tumor models *in vitro* and in clinical trials of patients with m*SDH* GIST.

Results: Molecular and metabolic characterization of our patient-derived m*SDH* GIST models revealed that these models recapitulate the transcriptional and metabolic hallmarks of parent tumors and SDH deficiency. We further demonstrate that temozolomide elicits DNA damage and apoptosis in our m*SDH* GIST models. Translating our *in vitro* discovery to the clinic, a cohort of patients with *SDH*-mutant GIST treated with temozolomide ($n = 5$) demonstrated a 40% objective response rate and 100% disease control rate, suggesting that temozolomide represents a promising therapy for this subset of GIST.

Conclusions: We report the first methods to establish patient-derived m*SDH* tumor models, which can be readily employed for understanding patient-specific tumor biology and treatment strategies. We also demonstrate that temozolomide is effective in patients with m*SDH* GIST who are refractory to existing chemotherapeutic drugs (namely, TKIs) in clinic for GISTs, bringing a promising treatment option for these patients to clinic.

See related commentary by Blakely et al., p. 3

Introduction

Gastrointestinal stromal tumor (GIST) is the most common sarcoma of the gastrointestinal tract. Although they are most frequently present in the stomach, they can arise anywhere in the GI tract (1). The majority of GISTs harbor oncogenic driver mutations in two receptor tyrosine kinases, namely, *KIT* and platelet-derived growth factor receptor alpha (*PDGFRA*). These *KIT*- or *PDGFRA*-mutant tumors are highly sensitive to tyrosine kinase inhibitors (TKI) such as imatinib and avapritinib, respectively, which are the mainstay of therapy for most patients with GIST (2). However, a distinct subset of GISTs (5%–7.5%) arise in the setting of Carney-Stratakis syndrome (also called Hereditary GIST-Paraganglioma syndrome), which results from inherited loss of function mutations in the genes encoding the succinate dehydrogenase (SDH) enzyme complex. These *SDH*-mutant GISTs, which are particularly common in children, adolescents, and young adults, are highly metastatic and have low TKI response rates (generally less than 15%; ref. 1).

The SDH enzyme complex consists of four subunits—SDHA, SDHB, SDHC, and SDHD—and plays central roles in cellular respiration and energy production. It is the only enzyme complex that participates in both the tricarboxylic acid (TCA) cycle and mitochondrial electron transport. GISTs and paragangliomas (PGL) with inactivating mutations in the *SDHA, SDHB, SDHC*, or *SDHD* genes lack a functional SDH complex (i.e., they are SDH deficient), resulting in elevated levels of an oncometabolite—succinate (3, 4). Intracellular accumulation of succinate causes metabolic and epigenetic rewiring with global DNA hypermethylation and gives SDH-deficient GIST a strikingly divergent biology from other GIST subtypes (5).

Modeling TKI-resistant SDH-deficient GIST is needed to find effective therapies for this patient population. Existing GIST models are primarily for *KIT*-mutant GISTs, while SDH-deficient GISTs have been difficult to model (6–9). Models for SDH-deficient tumors are

[1]Moores Cancer Center, University of California San Diego, La Jolla, California. [2]Department of Surgery, Division of Surgical Oncology, University of California San Diego, San Diego, California. [3]Department of Bioengineering, University of California San Diego, La Jolla, California. [4]Department of Medicine, Division of Hematology Oncology, University of California San Diego, San Diego, California. [5]Department of Radiation Medicine and Applied Sciences, University of California San Diego, San Diego, California. [6]Department of Radiology, Stanford University, Palo Alto, Stanford, California. [7]Department of Pathology, OHSU Knight Cancer Institute, Portland, Oregon. [8]Hematology/Medical Oncology, Portland VA Health Care System and OHSU Knight Cancer Institute, Portland, Oregon. [9]Center for Personalized Cancer Therapy, University of California San Diego Moores Cancer Center, San Diego, California. [10]Department of Medicine, Division of Biomedical Informatics, University of California San Diego, San Diego, California. [11]Diabetes and Endocrinology Research Center, University of California San Diego, La Jolla, California. [12]Institute of Engineering in Medicine, University of California San Diego, La Jolla, California.

Note: Supplementary data for this article are available at Clinical Cancer Research Online (http://clincancerres.aacrjournals.org/).

M. Yebra and S. Bhargava contributed equally to this article.

Corresponding Author: Jason K. Sicklick, Department of Surgery, Division of Surgical Oncology, University of California San Diego, San Diego, CA 92093. Phone: 858-822-6173; Fax: 858-228-5153; E-mail: jsicklick@health.ucsd.edu

Clin Cancer Res 2022;28:187–200

doi: 10.1158/1078-0432.CCR-21-2092

Translational Relevance

Gastrointestinal stromal tumors (GIST) with SDH deficiency often metastasize, are tyrosine kinase inhibitor–resistant, and affect adolescents and young adults. Currently, no consistent m*SDH* GIST models exist in the field, impeding their molecular characterization and drug screening. Our study introduces a novel pipeline for generation of patient-derived tumor models for m*SDH* GISTs for understanding pathobiology of the disease and for an application in personalized drug screening. These models were characterized, and they recapitulate parent tumor gene expression and metabolism. We demonstrate that temozolomide effectively reduced cell viability in our m*SDH* GIST models and showed promising results in our clinical trials, thus introducing a new drug in our arsenal against m*SDH* GISTs.

limited and the downstream effects of SDH-loss and succinate accumulation is primarily studied by knockdown or genetic depletion of SDH subunits in already established cell lines, murine or hamster cells (10–18). These models have accelerated our understanding of major pathways being affected; however, they often do not recapitulate the complete panel of patient-specific mutations and epigenetic alterations, pathway interactions and gene expression profiles. Patient-derived xenografts (PDX) have been utilized for SDH-deficient GISTs, but the length of time required for establishing this model limits its use for preclinical and high-throughput drug testing (19, 20). Attempts to generate long-term cultures from these PDXs have had limited success (19), underscoring the requirement of better patient-derived models for functional and mechanistic studies.

In this study, we describe the generation and characterization of patient-derived *SDH*-mutant GIST cellular models that harbor mutations in *SDHA, SDHB*, or *SDHC*. These models possess hallmarks of SDH complex loss (i.e., lack of SDHB protein expression, induction of hypoxia-regulated genes, and accumulation of succinate). We further validate our model for preclinical testing of drugs. We demonstrate that our established models are sensitive to temozolomide, an alkylating drug that showed promising results on patients with SDH-deficient PGL. Finally, we assessed the treatment efficacy of temozolomide in a cohort of patients with TKI-resistant SDH-deficient GIST and found a high rate of treatment response and improved disease control. Collectively, our results suggest the potential use of our models in basic and translational research of SDH-deficient GISTs.

Materials and Methods

Human GIST samples

After obtaining informed written consent from each subject or each subject's guardian, tumor and blood samples were collected from patients with GIST at the University of California, San Diego, CA (UCSD). All procedures and patient studies were approved by the UCSD Human Research Protections Program (IRB #181755, 141555, 181798) and Clinicaltrials.gov NCT02478931. This study was conducted in accordance with the Declaration of Helsinki, Belmont Report, and U.S. Common Rule.

Tumor dissociation and primary cell culture

GIST primary tumor cells were isolated from freshly resected human GISTs from patients who underwent surgery at UC San Diego Moores Cancer Center (San Diego, CA). Tumor fragments were cut into small (2–4 mm) pieces, transferred to a tube containing RPMI 1640 (Corning, 10-040-CM) and a proprietary enzyme mixture from the MACS human tumor dissociation kit (Miltenyi Biotec, 130-095-929). It was dissociated using the gentleMACS Dissociator (Miltenyi Biotec) following the manufacturer's instructions. Undigested tissue was removed by passing through a MACS SmartStrainer 70-μm filter and dissociated tumor cells were washed with RPMI 1640 and collected by centrifugation. Cell viability was assessed using 0.4% Trypan Blue and cell were counted using a TC20 Automated Cell Counter (Bio-Rad Laboratories). Dissociated tumor cells were plated on a T75 flask coated with an extracellular matrix derived from the human bladder carcinoma cell line HTB-9 (21). Cells were maintained in RPMI growth media containing 5% FBS (or FBS; Gibco, Thermo Fisher Scientific, 16000044), 1 mmol/L sodium pyruvate (Lonza, 13-115E), 1% MEM-NEAA (Gibco, 11140050), insulin (5 ng/mL; Sigma-Aldrich, I2643), EGF (10 ng/mL; Sigma-Aldrich, E9644) hydrocortisone (200 ng/mL; Sigma-Aldrich, H0888), SCF (50 ng/mL; Peprotech, 300-07), IGF-1 (10 ng/mL; Peprotech, 100-11), 1X B-27 Serum-Free Supplement (Thermo Fisher Scientific, 17504044), 1× Antibiotic-Antimycotic (Corning, 30-004-CI) and maintained at 37°C with 5% CO_2. *Mycoplasma* contamination testing was regularly performed by PCR reaction on cellular supernatants.

HTB-9 matrix–coated plates were prepared by growing HTB9 monolayer to confluency and lysing a confluent HTB-9 monolayer with 20 mmol/L ammonium hydroxide for 10–15 minutes at room temperature. The lysate was then aspirated off and the flask was rinsed three times with sterile PBS. HTB-9 matrix–coated plates were stored in PBS containing 2× antibiotic-antimycotic at 4°C until used.

Authentication of cell cultures

The human cell line authentication service of ATCC was used to confirm the unique identity of our patient-derived m*SDH* GIST cell models from established cell lines. Short tandem repeat (STR) DNA profiling was performed to examine nine highly polymorphic genetic markers (Supplementary Table S1) with genomic DNA from our m*SDH* GIST cell models. Comparative analysis was employed to compare the m*SDH* GIST models with all cell lines in the ATCC's STR Profile database and demonstrated no matching lines.

Cell lines

The GIST882 (KIT^{K642E}) line (RRID:CVCL_7044) was provided by S. Singer, Memorial Sloan-Kettering Cancer Center, New York, NY, and cultured in RPMI 1640 supplemented with 20% FBS (Sigma, F0926) and 1× antibiotic-antimycotic at 37°C with 5% CO_2.

HTB-9 cells were maintained in RPMI 1640 supplemented with 10% FBS (Gibco, Thermo Fisher Scientific, 16000044) maintained at 37°C with 5% CO_2.

GIST-T1 line [KIT exon 11 (V560-Y579Δ5: imatinib-sensitive] was provided by T. Taguchi, Kochi Medical School, Kochi, Japan and cultured in DMEM supplemented with 10% FBS (Sigma, F0926) and 1× antibiotic-antimycotic at 37°C with 5% CO_2.

Non-adherent spheroid culture

For the spheroid culture, m*SDH* GIST models were seeded at a density of 5×10^5 cells/well in 6% Poly(2-hydroxyethyl methacrylate; Poly-HEMA, Sigma-Aldrich, P3932). Poly-HEMA–coated 6-well plates in growth medium and allowed to grow as spheres for 3–7 days at 37°C with fresh media added every 3 days. Sphere formation was monitored using an EVOS cell imaging system (Thermo Fisher Scientific).

Soft agar colony formation and methylcellulose assay

Soft agar colony formation was performed by resuspending 2,000–16,000 cells/well of m*SDH* models in 0.4% agarose (SeaPlaque agarose; Lonza) in complete growth medium and seeded in 24-well plates precoated with 0.8% agarose (in complete growth medium) in triplicate. The cells were incubated at 37°C with 5% CO_2 for 2–5 weeks prior to staining with crystal violet. Five fields per well were imaged and colonies were counted. Each experiment consists of at least two biological replicates.

For methylcellulose assays, 3% methylcellulose stock solution (R&D Systems) was thawed at 4°C, adjusted to room temperature, and diluted to a final working concentration of 1% in complete growth medium. Cells were harvested and resuspended at a density of 50,000 cells/well in methylcellulose. The cell suspension was mixed well and added to a Poly-HEMA–coated 6-well plate in triplicate. The plates were incubated for 2–3 weeks in a 37°C incubator with 5% CO_2. Colonies were visualized using an inverted Olympus microscope and quantified by counting five fields (20×) in each well.

Western blotting

Whole-cell lysates were prepared from cells grown on Col I-coated 6-well plates with RIPA lysis buffer (100 mmol/L Tris pH 7.5, 150 mmol/L sodium chloride, 0.1% deoxycholate, 0.1% SDS) in the presence of protease inhibitors and scraped. The lysates were cleared by centrifugation at 14,000 rpm for 20 minutes and total proteins were measured using the BCA protein assay (Thermo Fisher Scientific). A total of 40 μg protein was boiled in reducing NuPAGE LDS Sample Buffer (Thermo Fisher Scientific) or Laemmli sample buffer (Bio-Rad) and resolved on a NuPAGE 4%–12% Bis Tris gel (Invitrogen, Thermo Fisher Scientific). Proteins were transferred to a polyvinylidene difluoride membrane, blocked, and incubated with a mouse mAb to SDHA (Santa Cruz Biotechnology, catalog no. sc-166909, RRID: AB_10611174), a mouse mAb to SDHB (Santa Cruz Biotechnology, catalog no. sc-271548, RRID:AB_10659104), a mouse mAb to HIF1A (Thermo Fisher Scientific, catalog no. MA1-516, RRID:AB_325431), or with a rabbit polyclonal antibody against HIF2A (Proteintech, catalog no. 26422-1-AP, RRID:AB_2880510) at 4°C overnight. An SDHA-specific band, an SDHB-specific band, and a HIF1A-specific band were revealed using a peroxidase-conjugated goat anti-mouse IgG (H+L; Jackson ImmunoResearch Laboratories, 1:10,000); a HIF2A-specific band was detected using a peroxidase-conjugated goat anti-rabbit IgG (H+L; Invitrogen) and the Pierce ECL Western blotting detection system (Thermo Fisher Scientific, catalog no. 32109). Alternatively, cells were plated on Col I-coated 6-well plates and treated with Vehicle (DMSO) or temozolomide (500 μmol/L) for 72 hours, lysed, and 10 μg protein was boiled in reducing Laemmli sample buffer and resolved on NuPAGE 4%–12% Bis Tris gels. Proteins were transferred and the membranes blocked, as described above, then probed with rabbit monoclonal antibodies against DR5 (Cell Signaling Technology, catalog no. 8074, 1:1,000, RRID:AB_10950817), p21 Waf1/Cip1 (Cell Signaling Technology, catalog no. 2947, 1:1,000, RRID:AB_823586), cleaved caspase 3 (Cell Signaling Technology, catalog no. 9661, 1: 500), MGMT (Cell Signaling Technology, catalog no. 2739, 1:500, RRID: AB_2297658), γ-H2AX (Cell Signaling Technology, catalog no. 2577, 1:1,000), and α-tubulin (Cell Signaling Technology, catalog no. 3873, 1:5,000) at 4°C overnight, followed by detection using appropriate peroxidase-conjugated secondary antibodies and ECL as described above.

Immunofluorescence and confocal microscopy

m*SDH* GIST cells that had been expanded on a matrix-coated plate as described above were plated on Col I-coated chamber slides overnight and fixed with 4% paraformaldehyde/PBS for 20 minutes. Fixed cells were permeabilized for 5 minutes with 0.3% Triton X-100 in PBS, then blocked with PBS/5% normal donkey serum for 1 hour, and stained with a polyclonal rabbit anti-human c-KIT antibody (Dako, catalog no. A4502, 1:600) and a mouse monoclonal antibody against DOG-1 (Santa Cruz Biotechnology, catalog no. sc-377115, 1:100) diluted in blocking buffer overnight at 4°C. Slides were then incubated with Alexa Fluor-conjugated secondary antibodies (AF594 or AF488) specific for mouse and rabbit (Thermo Fisher Scientific) and1 μg/mL DAPI (4′,6-diamidino-2-phenylindole) for 1 hour at room temperature in the dark, washed, and mounted in ProLong Gold antifade mounting medium (Invitrogen, Thermo Fisher Scientific). Immunofluorescence staining was imaged on a Nikon Eclipse C1 confocal microscope with a 1.4 NA 60× oil-immersion lens. Alternatively, tumor cells were allowed to grow for 7 days as tumorspheres on 6% poly-HEMA–coated 6-well plates, then pelleted, embedded in optimal cutting temperature (OCT), and sectioned. Sections were fixed and stained as described above. Patient tumors were embedded in OCT, sectioned, and processed as described for tumorspheres above. To measure SDHB expression, m*SDH* GIST cells were cultured on Col I-coated chamber slides, fixed, permeabilized and blocked as described above, and stained with a mouse mAb to SDHB (Santa Cruz Biotechnology, catalog no. sc-271548, 1:200, RRID:AB_10659104) at 4°C overnight, washed, and stained with a donkey anti-mouse IgG (H+L)Alexa Fluor 488 antibody (Thermo Fisher Scientific, 1:1,000) and 1 μg/mL DAPI in 5% NDS in PBS for 1 hour at room temperature in the dark, washed, and mounted in ProLong Gold antifade mounting medium. Images were taken with a Keyence BZ-X710 fluorescence microscope (Keyence Corporation).

To measure the levels of DNA methylation, tumorspheres were stained with a rabbit mAb against 5-methylcytosine (Cell Signaling Technology, catalog no. 28692, 1:1,600, RRID:AB_2798962) or with a mouse mAb against 5-hydroxymethylcytosine (Cell Signaling Technology, catalog no. 51660, 1:200, RRID:AB_2799398) followed by staining with their respective Alexa Fluor 488 or Alexa Fluor 594-conjugated secondary antibodies according to supplier instructions.

To measure DNA damage, cells were plated on Col I-coated chamber slides and treated with either vehicle (DMSO) or temozolomide for 72 hours washed with PBS, fixed with 2% paraformaldehyde (w/v) in PBS for 15 minutes, washed, and permeabilized in 0.5% Triton X-100 in PBS for 10 minutes. Following three washes with PBS, cells were stained with a primary antibody against γ-H2AX (Cell Signaling Technology, catalog no. 2577, 1:500, RRID:AB_2118010) at 4°C overnight. Cells were washed and stained with a donkey anti-rabbit IgG (H+L) Alexa Fluor 594 antibody (Thermo Fisher Scientific, 1:1,000) and 1 μg/mL DAPI in 5% NDS in PBS for 1 hour at room temperature in the dark. Mounting was performed as described above. Images were taken with a Keyence BZ-X710 fluorescence microscope.

RNA isolation for RNA sequencing

Total RNA was isolated from homogenized, snap-frozen human GISTs and from the corresponding cell cultures using the RNeasy Kit from Qiagen according to manufacturer's instructions. DNase-treatment was performed using the RNase-Free DNase Set from Qiagen to remove contaminating DNA. RNA concentrations were determined using the NanoDrop 2000c (Thermo Fisher Scientific) and RNA quality was assessed using an Agilent Tapestation; samples

determined to have an RNA integrity number of ≥7 were used. Libraries were generated at the UC San Diego Institute for Genomic Medicine (IGM) Genomics Center from 1 μg of total RNA using Illumina's TruSeq Stranded mRNA Sample Prep Kit. Libraries were pooled and sequenced with 100 bp paired end reads (PE100) to a depth of approximately 25 million reads per sample on an Illumina HiSeq2500 Instrument. Genome alignment was performed by STAR aligner with the human genome (hg38).

qRT-PCR

Total RNA was isolated from adherent monolayers of GIST882, SD-437A, SD-424B, and SD-435C GIST cells using the RNeasy Kit (Qiagen), followed by DNase treatment. RNA concentration was determined using the NanoDrop 2000c as described above. cDNA was synthesized by reverse transcription using the iScript cDNA Synthesis Kit (Bio-Rad Laboratories) in a 40 μL reaction using 2 μg of total RNA. Real-time PCR was carried out on the CFX96 Real-Time Thermal Cycler (Bio-Rad) using the iTaq Universal SYBR Green Supermix (Bio-Rad). Expression relative to a reference housekeeping gene and fold change was calculated relative to *SDH*-WT (wildtype) GIST cells using the $2^{-\Delta\Delta C_t}$ method (22). Primer sequences are listed in Supplementary Table S2. Primer sequences were obtained from either a published study (23), or the Harvard PrimerBank publicly available database (24), or when not available, designed using Invitrogen primer design and primer3 tools (25).

Genomic analysis of patient tumors and cell cultures

DNA extracted from formalin-fixed paraffin-embedded sections of patient tumors was used to make hybridization-captured, adaptor ligation-based libraries. As part of routine clinical care, all tumors were sequenced by Foundation Medicine, Inc. using The FoundationOne assay, a next-generation sequencing (NGS)-based genomic assay that utilizes the Illumina HiSeq 2500 instrument (Illumina Inc.) to sequence coding regions of more than 400 cancer-related genes (including SDHx). Total DNA was extracted from m*SDH* GIST cell cultures using the Wizard DNA isolation Kit as described above. NGS of these cell cultures was performed at the Oregon Health Sciences University (OHSU) Knight Diagnostics Laboratory (Portland, OR) for SD-437A, SD-424B, and SD-435C.

Measurement of cell viability

Cells were harvested from an extracellular matrix-coated plate (either HTB9 or Col I) with TrypLE Express (Gibco, 12605028) and m*SDH* models were seeded at 600–1,000 cells/well in Col IV-coated Corning 96-well black polystyrene TC-treated microplates (Sigma-Aldrich, CLS3904,), allowed to attach overnight, and then treated with 10–11 doses of the indicated compounds for 3–7 days. Drugs used include temozolomide (Selleckchem, S1237), 2-deoxy-D-glucose (Selleckchem, 25972), 6-aminonicotinamide (Thermo Fisher Scientific, AAL0669203), imatinib (Chemietek), and sunitinib malate (Thermo Fisher Scientific, 341031-54-7 RS046). DMSO was used as a vehicle at the appropriate concentration. Cell viability was determined using the CellTiter-Glo Cell Viability Assay kit (Promega Corporation, G7572) according to manufacturer protocols. Data were expressed as percentages of the survival of vehicle-treated control cells.

For Methyl-tetrazolium (MTT) assay, GIST-T1 and GIST882 cells were seeded in 96-well plate and treated with imatinib or sunitinib for 72 hours. MTT reagent, 3-(4, 5-dimethylthiazol-2-yl)-2,5- diphenyltetrazolium bromide (Sigma) was added and cells were incubated with the reagent for 4 hours at 37°C. DMSO was added to dissolve the formazan crystals. The absorbance was read at 570 nm and percentage viability compared to the DMSO control wells was determined.

Comet tail assay for DNA damage

Temozolomide-induced DNA double-strand breaks (DSB) were measured using neutral comet tail assay. Briefly, 2.5×10^5 cells were plated in Col I-coated T25 flasks overnight, then treated for 72 hours with either vehicle or 500 μmol/L temozolomide. Cells were then harvested and assayed using the Trevigen CometAssay kit (Trevigen) following the manufacturer's instructions. Comet tail length in pixels was measured using CometScore freeware (TriTek Corp.) as described previously (26). About 100–150 cells were analyzed in each sample group.

Tracing/metabolomics experiments

KIT-mutant and m*SDH* GIST patient plasma samples were obtained from the UC San Diego Moores Cancer Center Biorepository and Tissue Technology Shared Resource. Plasma metabolites were extracted from *KIT*-mutant and *SDH*-mutant GIST patient plasma samples and quantified as follows. For metabolite extraction, 10 μL of each plasma sample was utilized. First, 90 μL of a 9:1 methanol water mix was added to each sample and the samples were vortexed for 1 minute. After centrifugation at 16,000 × *g* for 10 minutes, 90 μL of supernatant was collected, evaporated under vacuum at −4°C, and analyzed using gas chromatography/mass spectrometry (GC-MS). Metabolite levels of succinate were quantified using external standard curves (three biological replicates). Metabolites were extracted from subconfluent WT (GIST882) and m*SDH* (SD-437A, SD-424B, and SD-435C) GIST cells (200,000) cultured under attached conditions for 24 hours in glutamine-free RPMI 1640 medium containing 2 mmol/L [U-$^{13}C_5$]-glutamine, 11 mmol/L glucose, and 5% FBS (Gibco). Metabolites were extracted using a modified Bligh and Dyer method using methanol/chloroform/water as described previously (27).

GC-MS sample preparation and analysis

GC-MS sample preparation and analysis were performed as described previously (Cordes). Briefly, polar metabolites were derivatized using a Gerstel MultiPurpose Sampler (MPS 2XL). Methoxime-tBDMS derivatives were formed by addition of 15 μL 2% (w/v) methoxylamine hydrochloride (MP Biomedicals) in pyridine and incubated at 45°C for 60 min. Samples were then silylated by addition of 15 μL *N*-tert-butyldimethylsily-*N*-methyltrifluoroacetamide (MTBSTFA) with 1% tert-butyldimethylchlorosilane (tBDMS; Regis Technologies) and incubated at 45°C for 30 minutes. Derivatized samples were injected into a GC-MS using a DB-35MS column (30 m × 0.25 mm inner diameter × 0.25 μm, Agilent J&W Scientific) installed in an Agilent 7890B GC system integrated with an Agilent 5977a MS. Samples were injected at a GC oven temperature of 100°C which was held for 1 minute before ramping to 255°C at 3.5°C/minute, then to 320°C at 15°C/minute, and held for 3 minutes. Electron impact ionization was performed with the MS scanning over the range of 100–650 m/z. Metabolite levels and mass isotopomer distributions of derivatized fragments were analyzed with an in-house Matlab script which integrated the metabolite fragment ions and corrected for natural isotope abundances.

Respiration experiments

Respiration measurements on adherent monolayers of GIST882, SD-437A, SD-424B, SD-435C GIST cells were performed using a Seahorse XF96 Analyzer. Briefly, cells were plated at 25,000 cells/well 48 hours before measurement. Intact cells were assayed in DMEM

(Sigma, #5030) supplemented with 8 mmol/L glucose, 2 mmol/L glutamine, 2 mmol/L pyruvate, and 2 mmol/L HEPES. Cells were permeabilized with 3 nm perfringolysin O (commercially XF PMP) as described previously (28). State 3, succinate-driven respiration was measured in permeabilized cells offered 4 mmol/L ADP, 2 μmol/L rotenone, and 5 mmol/L succinate. NADH-driven respiration was measured in permeabilized cells offered 4 mmol/L ADP, 5 mmol/L pyruvate, and 0.5 mmol/L malate. Maximal respiration was calculated as the difference between protonophore-stimulated respiration (600 nmol/L FCCP) and nonmitochondrial respiration (measured after addition of 1 μmol/L antimycin A). Data were normalized to protein content using the Pierce BCA assay.

Patient response

Tumor responses to treatment were assessed by RECIST version 1.1 and PERCIST (29, 30).

Gene expression analysis

The gene expression level were obtained by processing the RNA-sequencing reads through the BCBIO-nextGen pipeline (31), including alignment with STAR aligner (32) and isoforms expression using Salmon (32) and gene level expression using the featureCount script. The expression counts were then processed using DESeq (33) including variance stabilization with rlog transformation.

Gene set enrichment analysis

The level of activity of each gene set investigated (Supplementary Fig. S2E) was calculated using single sample gene set enrichment analysis (GSEA) implemented in the GSVA R package (method = "ssgsea"). Enrichment scores were then scaled to the 0–1 range.

Data analysis and statistical analysis

Half maximal inhibitory (IC_{50}) concentration values of compound data were calculated using Prism software (GraphPad Software, RRID: SCR_002798). All values are expressed as the mean ± SD ($n = 3$), unless otherwise noted. For the statistical analyses, results were analyzed using Mann–Whitney *t* test when indicated or one-way ANOVA followed by the Student *t* test, and Sidak multiple comparison test to compare among more than two groups. Differences were considered statistically significant if $P < 0.05$.

Results

Establishment of patient-derived mutant *SDH* GIST models

We obtained *SDH*-mutant tumor tissue from patients who underwent surgical resection under an Institutional Review Board–approved protocol following informed consent. Tumors representative of each mutated SDH subunit were utilized for this study (described below). Single cells from freshly resected tumors were obtained using a combination of mechanical and enzymatic dissociation (**Fig. 1A**). We experimented with a variety of media compositions and culture conditions. From our observation, these cells could only grow for limited passages on regular culture dishes. Because extracellular matrices have been demonstrated to promote the growth and expansion of tumor cells *in vitro* (34), we examined whether m*SDH* GIST cells could proliferate on an extracellular matrix. We determined that our m*SDH* models [designated as SD-437A (*SDHA* splice site 1432_1432+1delGG), SD-424B (*SDHB* R90*), and SD-435C (*SDHC* R133*) where the A, B, or C refers to the mutated *SDH* gene] could propagate in two-dimensional (2D) cultures on a laminin-rich matrix derived from the HTB9 bladder carcinoma cell line (**Fig. 1B**; ref. 21). In our current media composition and extracellular matrix, we are able to maintain these models for around 20 passages under normoxia. Unique identity of these cells was confirmed by STR cell line authentication (Supplementary Table S1). These cells further demonstrated anchorage independence and were able to grow in non-adherent conditions as spheroids in three-dimensional (3D) suspensions (after 7 days) (**Fig. 1B**), as well as form colonies in soft agar (at 3–5 weeks; Supplementary Fig. S1A and 1B) and in 1% methylcellulose (after 2 weeks; Supplementary Fig. S1C and S1D).

We next interrogated whether these established m*SDH* GIST models recapitulate the metabolic, transcriptomic, and proteomic characteristics of parental tumors. GISTs are characterized by the expression of two diagnostic markers, namely, KIT and DOG-1 (7, 35). First, we confirmed the expression of these markers in parental tumors and our m*SDH* GIST models. An established *KIT*-mutant GIST cell line (GIST882), which is WT for *SDH*, was used as a positive control as the media conditions are similar to those of the m*SDH* GIST models. Parental tumors and derived matched primary models grown in adherent and non-adherent conditions expressed both KIT and DOG-1 (**Fig. 1C**). SDH-deficient GISTs, which include tumors harboring mutant or epigenetically silent *SDH* subunits have undetectable levels of *SDHB* protein. This loss of *SDHB* protein expression in our models was confirmed by immunoblotting (**Fig. 1D**) and immunofluorescent staining (**Fig. 1E**). In contrast, SDHA protein levels were unaltered except in the m*SDHA* cells as expected (**Fig. 1D**). Collectively, our models recapitulate the expression of characteristic markers of GIST tumors and have SDHB loss characteristic of SDH-deficient GISTs.

Mutant *SDH* GIST models mimic central carbon metabolic defects of SDH-deficient GISTs

The mitochondrial SDH complex in the Krebs cycle catalyzes the oxidation of succinate to fumarate. To assess whether inactivation of SDH complex in SDH-deficient GIST affects central carbon metabolism, we interrogated matched patient plasma samples from patients whose tumors were used for establishing our cell models and performed a targeted metabolomic analysis. Significantly elevated succinate plasma concentrations and succinate/fumarate ratios were observed in SDH-deficient GIST patient plasma compared with SDH-proficient GIST patient plasma (Supplementary Fig. S2A and S2B). We next interrogated whether our human m*SDH* GIST models mimic these metabolic alterations. Indeed, our models had elevated succinate levels (**Fig. 2A**) and elevated succinate/fumarate ratios (**Fig. 2B**) as compared with WT-*SDH* cells. As we confirmed, the abrogation of a crucial step in the TCA cycle and subsequent alterations in TCA cycle intermediates, we next investigated mitochondrial activity of our models relative to WT-*SDH* GIST cells. All m*SDH* GIST models have diminished basal and maximal uncoupled respiration relative to WT-*SDH* cells in Seahorse assays (**Fig. 2C** and **D**). A reduction in both Complex I and Complex II-mediated oxygen consumption rates (OCR) in permeabilized cells was also observed, indicative of mitochondrial dysfunction (**Fig. 2E**). In addition, these cells exhibit a pseudohypoxic metabolic phenotype, with increased reductive carboxylation, as indicated by elevated α-ketoglutarate/citrate levels (**Fig. 2F**) and increased M5 citrate labeling from [U-$^{13}C_5$]glutamine (**Fig. 2G–H**). These results are consistent with reports of increased reductive carboxylation, as well as expression and flux through pyruvate carboxylase in immortalized mouse chromaffin cell lines isolated from *Sdhb* knockout mice (36, 37). In addition, metabolic tracing studies revealed that impaired SDH activity led to increased glycolysis, as indicated by increased M3 pyruvate

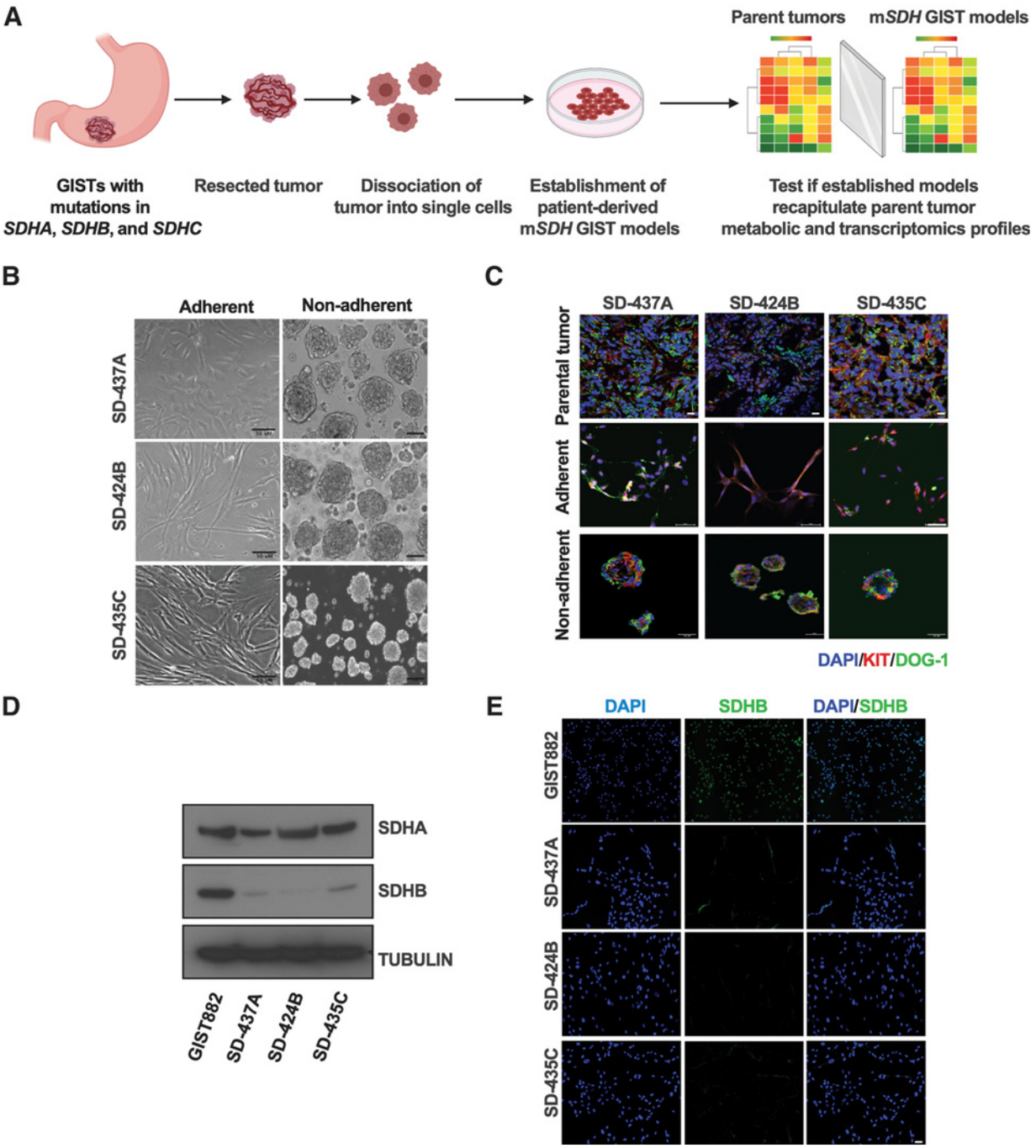

Figure 1.

Establishment and characterization of *SDHA-, SDHB-, and SDHC*-mutant human GIST models. **A,** Schematic representation of workflow of establishment of patient-derived m*SDH* GIST models and validation for recapitulation of essential features of parent tumors. **B,** Micrographs of m*SDH* GIST models SD-437A, SD-424B, and SD-435C propagated in adherent conditions on a laminin-rich HTB9 matrix (2D) or in non-adherent conditions for 7 days as spheroids on Poly-HEMA–coated wells (3D). Scale bar, 50 μm. **C,** Immunofluorescence staining of KIT (red) and DOG-1 (green) in parent tumors and m*SDH* GIST models grown in adherent and in non-adherent conditions. **D,** Immunoblot analysis confirming expression of SDHA and SDHB protein in *KIT*-mutant/*SDH*-WT (wildtype) GIST882 cells and in m*SDH* GIST models. α-tubulin was used as a loading control. **E,** Immunofluorescence staining of SDHB (green) and DAPI (blue) in *KIT*-mutant/*SDH*-WT (wildtype) GIST882 cells and in m*SDH* GIST models. Scale bar, 50 μm.

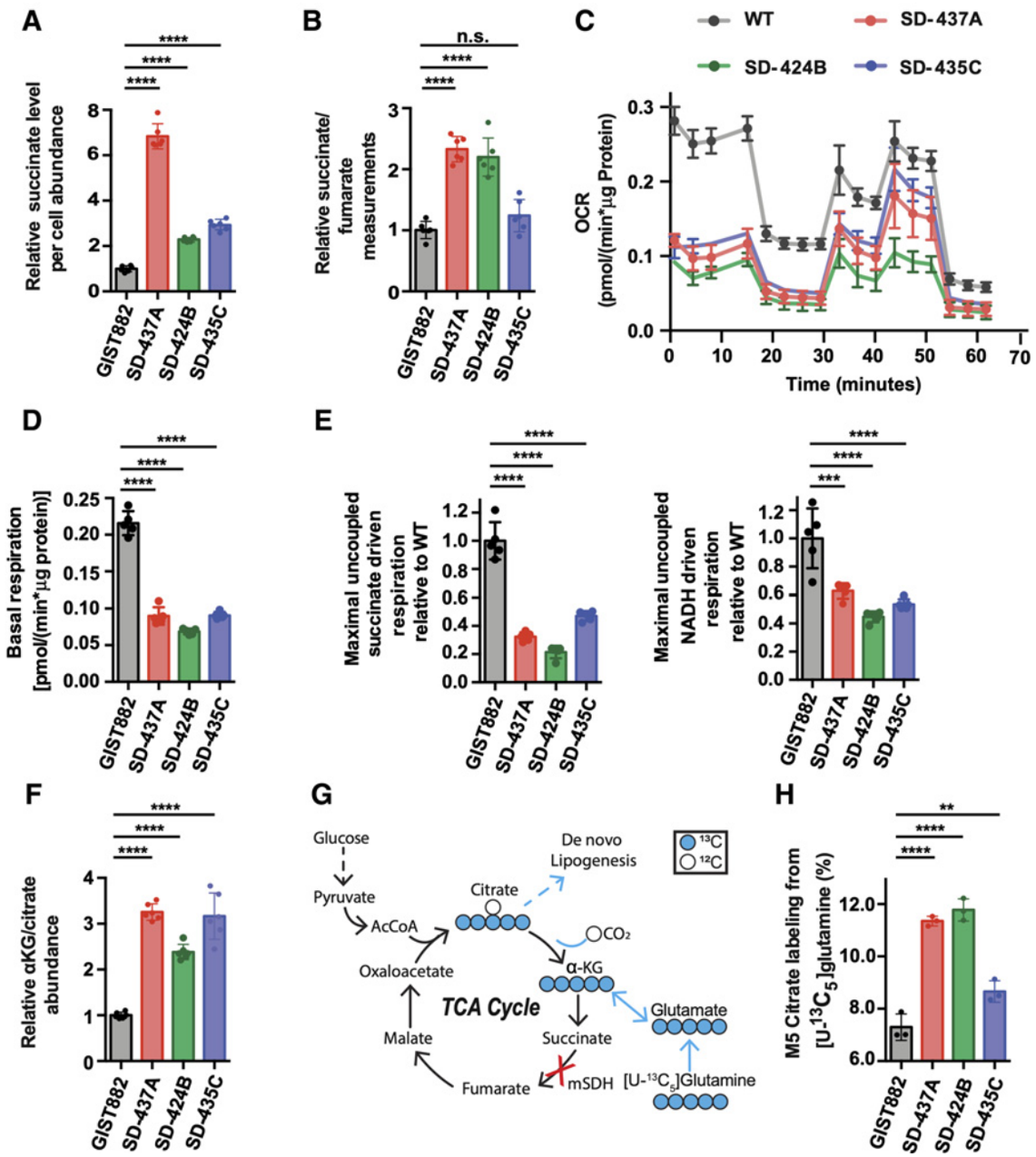

Figure 2.

Metabolic profiles of m*SDH* GIST models recapitulate SDH deficiency. **A,** Per cell abundance of succinate relative to GIST882 in m*SDH* GIST models grown for 48 hours ($n = 3$). One-way ANOVA (multiple comparisons) was performed for statistical analysis with ****, $P < 0.0001$. **B,** Ratio of intracellular succinate-to-fumarate concentrations relative to GIST882 in m*SDH* GIST models grown for 48 hours ($n = 3$). One-way ANOVA (multiple comparisons) was performed for statistical analysis with $P > 0.05$ (ns), ****, $P < 0.0001$. **C,** OCR trace of intact m*SDH* GIST models ($n = 5$). **D,** Basal respiration rate of intact m*SDH* GIST models ($n = 5$). One-way ANOVA (multiple comparisons) was performed for statistical analysis with ****, $P < 0.0001$. **E,** Maximal uncoupled respiration driven by succinate relative to WT in permeabilized m*SDH* GIST models ($n = 5$). One-way ANOVA was performed. ***, $P < 0.001$; ****, $P < 0.0001$. Maximal uncoupled respiration driven by NADH relative to WT in permeabilized m*SDH* GIST models ($n = 5$). One-way ANOVA was performed. ***, $P < 0.001$; ****, $P < 0.0001$. **F,** Ratio of intracellular α-KG to citrate relative to GIST882 in m*SDH* GIST models grown for 48 hours ($n = 3$). **G,** Atom transition diagram of reductive glutamine catabolism using a [U-$^{13}C_5$] glutamine tracer. Open circles represent ^{12}C, closed circles represent ^{13}C carbon atoms. **H,** Percent labeling of M5 citrate from [U-$^{13}C_5$]-glutamine in m*SDH* GIST models grown for 48 h ($n = 3$). Data are represented as mean ± SEM, with biological replicates as indicated. One-way ANOVA was performed for statistical analysis, with $P > 0.05$ (ns); *, $P < 0.05$; **, $P < 0.01$; ***, $P < 0.001$; ****, $P < 0.0001$.

(Supplementary Fig. S2C) and M3 lactate (Supplementary Fig. S2D) labeling from [U-$^{13}C_6$]glucose. This is consistent with increased glucose oxidation. Finally, the m*SDH* GIST models also showed higher levels of 2-hydroxyglutarate (2-HG) than WT-*SDH* cells (Supplementary Fig. S2E).

Our metabolic tracing studies revealed that m*SDH* models had increased glycolysis, which compelled us to test whether inhibition of glucose metabolism with either 2-deoxy-D-glucose (2-DG; a glycolysis inhibitor) or 6-aminonicotinamide (6-AN; a pentose phosphate pathway inhibitor) would impact the growth of these cells. Indeed, treatment with either inhibitor resulted in significantly decreased cell viability in a dose-dependent fashion (Supplementary Fig. S2F and S2G). This is consistent with earlier reports showing that inhibition of glycolysis in GIST cell lines inhibits cell viability (38). Together, our findings demonstrate that m*SDH* models, which have decreased respiratory activity and impaired mitochondrial function, are dependent upon glycolysis for survival.

Epigenetic and transcriptional alterations in m*SDH* GIST models are consistent with SDH deficiency

Tumor heterogeneity, cell–cell interactions, and cell–extracellular matrix interactions within the tumor microenvironment are critical for tumor growth and chemoresistance. To characterize our models further, we next defined the transcriptional profiles of our patient-derived m*SDH* GIST models and matched parental tumors. RNA sequencing of patient tumors and corresponding m*SDH* GIST models revealed a greater than 90% concordance between gene expression in the tumors and their derived cell models, reflecting minimal alterations of gene expression under our cell culture conditions (**Fig. 3A**) as reported in recent GBM models (39). Next, we compared the gene

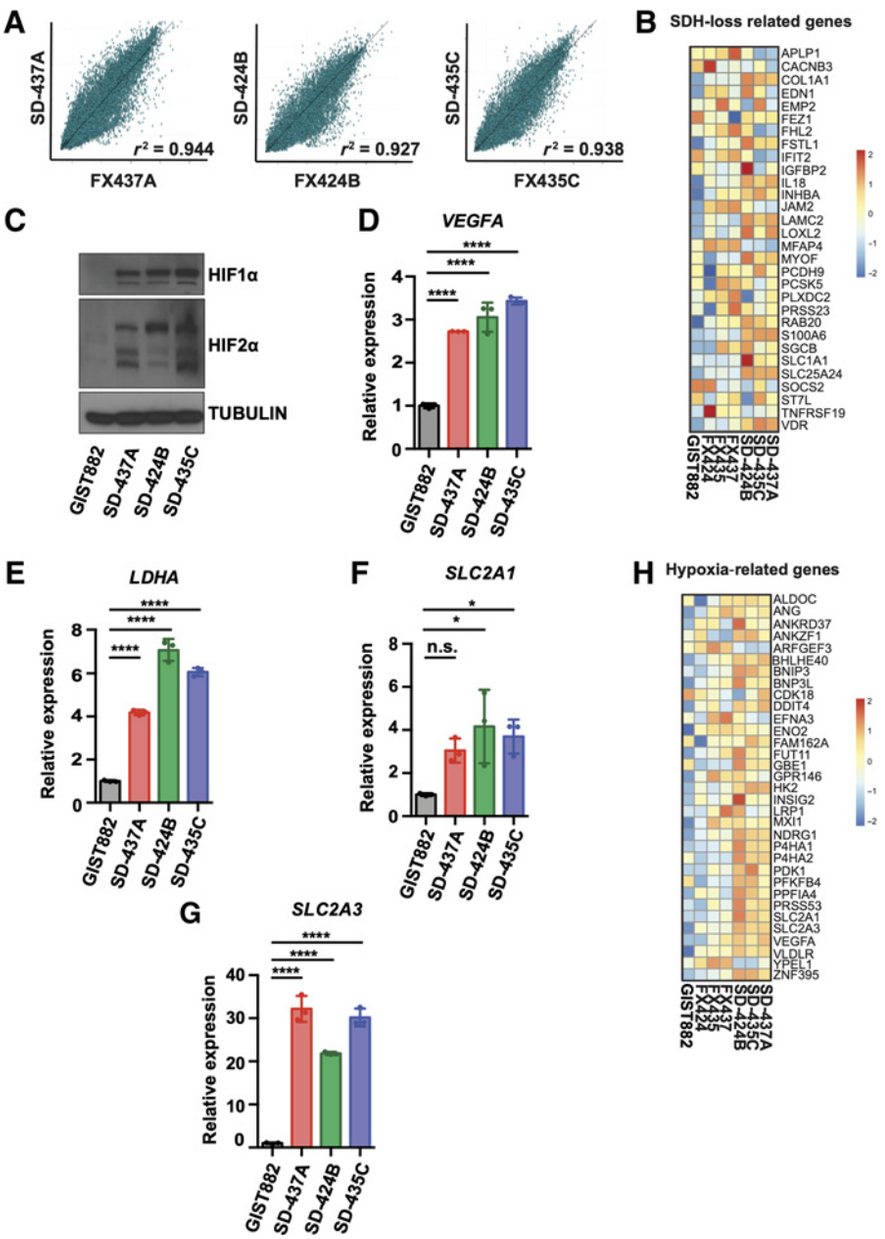

Figure 3.

Transcriptional profiles of m*SDH* GIST models recapitulate SDH deficiency. **A,** Scatterplots comparing gene expression levels (RNA sequencing) between patient tumors (*x*-axis) and m*SDH* GIST models (*y*-axis) as measured by Pearson correlation coefficient ($r^2 > 0.9$). **B,** The relative expression levels (z-scores) for each gene comprising SDH loss related gene set (40) are indicated for each SDH-deficient tumor and models, as well as one WT *SDH* (non–SDH-deficient) cell line (GIST882). **C,** Immunoblot of HIF1α and HIF2α proteins in *KIT*-mutant/*SDH*-WT (wildtype) GIST882 cells and in m*SDH* GIST models. qPCR analysis of *HIF1A* target gene *VEGFA* (**D**), LDHA (**E**), SLC2A1 (**F**), and SLC2A3 (**G**) expression in m*SDH* GIST models. Results are depicted as fold-change relative to WT-*SDH* (GIST882) cells. One-way ANOVA was performed for statistical analysis with $P > 0.05$ (ns); *, $P < 0.05$; ****, $P < 0.0001$. **H,** The relative expression levels (z-scores) for each gene comprising the hypoxia-related gene set (43) are indicated for each SDH-deficient tumor and models, as well as one WT *SDH* (non–SDH-deficient) cell line (GIST882).

profiles of the matched tumors and cell cultures with published gene sets for SDH-deficient tumors and cell. We observed an enrichment of transcripts overexpressed in an *SDHB*-silenced human hepatocellular carcinoma cell line (40), including genes involved in cell adhesion (*LAMC2, COL1A1*), proliferation (*INHBA*), and metabolic processes (*SLC1A1*; **Fig. 3B**).

Our earlier observations demonstrated that metabolic rewiring in SDH-deficient tumors leads to accumulation of succinate. Succinate inhibits α-ketoglutarate (α-KG)-dependent dioxygenases, including the HIF-prolyl 4-hydroxylases for hypoxia-inducible factor (HIF), which results in stabilization of HIF and in a "pseudo-hypoxic" state, that leads to upregulation of HIF-dependent targets (11, 15, 41, 42). Consistently, our m*SDH* GIST models exhibited elevated protein levels of HIF1α and HIF2α as compared with a WT-*SDH* GIST cell line (**Fig. 3C**). HIF1α target genes, including *LDHA, VEGFA, SLC2A1*, and *SLC2A3* were also found to be higher in m*SDH* models than WT-*SDH* GIST cell line (**Fig. 3D–G**). Finally, we observed that HIF1 signaling genes (e.g., *VEGFA, SLC2A1, SLC2A3, HK2*, and *ENO2)* previously linked to a hypoxia signature in soft tissue sarcomas (43) were also highly expressed in these resected tumors and primary cell cultures (**Fig. 3H**). Gene expression and GSEA confirmed that the normalized gene expression levels seen in our SDH-deficient tumors and cells were higher than those found in a WT-*SDH* GIST line (Supplementary Fig. S3A and S3B). SDH-deficient GISTs and PGLs have higher levels of 5-methylcytosine (5-mC) as compared with 5-hydroxymethylcytosine (5-hmC), resulting in global gene hypermethylation. Similarly, our m*SDH* models also express higher levels of 5-mC compared with 5-hmC, as assessed by immunofluorescence (Supplementary Fig. S3C). Taken together, our findings confirm that these human SDH-deficient cell models have gene expression patterns commonly associated with SDH deficiency, hypoxia, and cancer metabolism.

TKI-resistant m*SDH* GIST models are sensitive to temozolomide-induced DNA damage

To further assess the validity of our m*SDH* GIST cell cultures as a human-derived model of TKI-resistant SDH-deficient GIST, we treated cells with imatinib and sunitinib (**Fig. 4A** and **4B**). Cell viability was only decreased at the highest concentrations of each drug, although they are known to be highly effective against *KIT*-mutant cell lines at lower doses (Supplementary Fig. S4A and S4B). Temozolomide has been used as an alkylating agent for metastatic pheochromocytoma and PGL (mPHEO/PGL; refs. 44, 45). This prompted us to examine whether our m*SDH* GISTs are sensitive to temozolomide. Indeed, temozolomide caused a dose-dependent reduction of cell viability in all m*SDH* GIST models (**Fig. 4C**). Temozolomide induces methyl adducts like O^6-meG, N^7-methylguanine (N^7-meG), and N^3-methyladenine (N^3-meA), resulting in DNA base mismatch repair with strand breaks (46). We next examined whether temozolomide would induce on-target DNA DSBs, as has been reported in human glioma cells (47). We treated cells for 72 hours with temozolomide or vehicle and measured DNA fragmentation using the neutral comet assay. We found that temozolomide significantly increased comet tail lengths in all the m*SDH* models (*A/B/C*) tested (**Fig. 4D**). Furthermore, γ-H2AX (phospho-S139 on histone H2AX), a marker for activated DNA damage response, increased after temozolomide treatment in m*SDH* GIST models (**Fig. 4E**), confirming that temozolomide suppresses cell viability by inducing on-target DNA damage.

We investigated the mechanism by which temozolomide may be causing a reduction in cell viability in our models. Temozolomide treatment induced p21, a cell-cycle arrest marker in our m*SDH* GIST models, which may be leading to a cell-cycle arrest in our models post treatment (**Fig. 4F**). Temozolomide also induced the expression of death receptor 5 (DR5) upon treatment, a molecule involved in extrinsic pathway of apoptosis (**Fig. 4F**). Our observations suggest that temozolomide may sensitize these models to TNF-related apoptosis-inducing ligand (TRAIL) therapy and this strategy can be further explored for m*SDH* tumors. Our earlier observations of temozolomide-induced DNA damage led us to interrogate the levels of MGMT, an enzyme involved in repairs of O^6-meG DNA adducts caused by temozolomide treatment. Promoter hypermethylation of O^6-methylguanine-DNA-methyltransferase (MGMT) is associated with temozolomide sensitivity (48, 49), while acquired temozolomide resistance is associated with increased MGMT expression (50–52). We investigated the levels of MGMT after temozolomide treatment in m*SDH* GIST models. Temozolomide treatment reduced the expression of MGMT in m*SDH* GIST models at 7 days while simultaneously increasing γ-H2AX (**Fig. 4G**). Furthermore, occurrence of apoptosis was confirmed by observation of cleaved caspase 3 (CC3) in temozolomide-treated m*SDH* GIST models, with the most dramatic effect in the m*SDHC* cells (**Fig. 4G**). Collectively, temozolomide decreased the expression of essential base excision repair protein, leading to further enhancement of DNA damage after treatment, which may be leading to reduced cellular viability.

Clinical efficacy of temozolomide in patients with TKI-resistant SDH-deficient GIST

At present, there are limited therapeutic options for patients with SDH-deficient GIST. In light of our findings that patient-derived m*SDH* GIST models are sensitive to temozolomide, we retrospectively analyzed five patients with widely metastatic SDH-deficient GIST treated with temozolomide at our institution from 2016 to 2018. The patients included 2 females and 3 males, with a median age of 29.7 years old (range: 22.4–44.3) at the start of temozolomide treatment. All patients had biopsy-proven SDH-deficient GIST and confirmed germline alterations in *SDHA* ($n = 1$), *SDHB* ($n = 2$), *SDHC* ($n = 1$), or ($n = 1$). Overall, they had received a median of one prior line of TKI therapy (range: 0–2). Having limited therapeutic options to offer these patients, they were treated with temozolomide (administered in 4-week cycles at 85 mg/m^2 daily for 21 days followed by 7 days off treatment). According to RECIST version 1.1 and/or PERCIST measurements (29, 30), the disease control rate, defined as partial response (PR) or stabilization of progressing disease, was 100% following treatment; two patients had radiologic PRs and three had stabilization of their disease (stable disease) following progression (**Fig. 5A–F**). Despite either low-volume metastatic disease (**Fig. 5A** and **B**) or very high-volume metastatic disease (**Fig. 5C** and **D**; Supplementary Fig. S5A and S5B), PRs were observed. The median overall survival (OS) from date of diagnosis was 6.4 years [95% confidence interval (CI), 0.9–13.6], and the median OS from the start of treatment was 1.9 years (95% CI, 0.07–1.2), suggesting that 4 of 5 patients had highly aggressive disease biology at the start of temozolomide treatment (**Fig. 5G** and **H**). Collectively, our observations suggest temozolomide to be a promising therapy for SDH-deficient GIST patient population.

Discussion

SDH mutations are present in multiple tumors including SDH-deficient GISTs, PGLs, pheochromocytomas (PCC), renal cell carcinomas, pituitary adenomas, thyroid tumors, and neuroblastomas. SDH-deficient GIST is an orphan disease with limited treatment options and limited applicable human models to facilitate drug

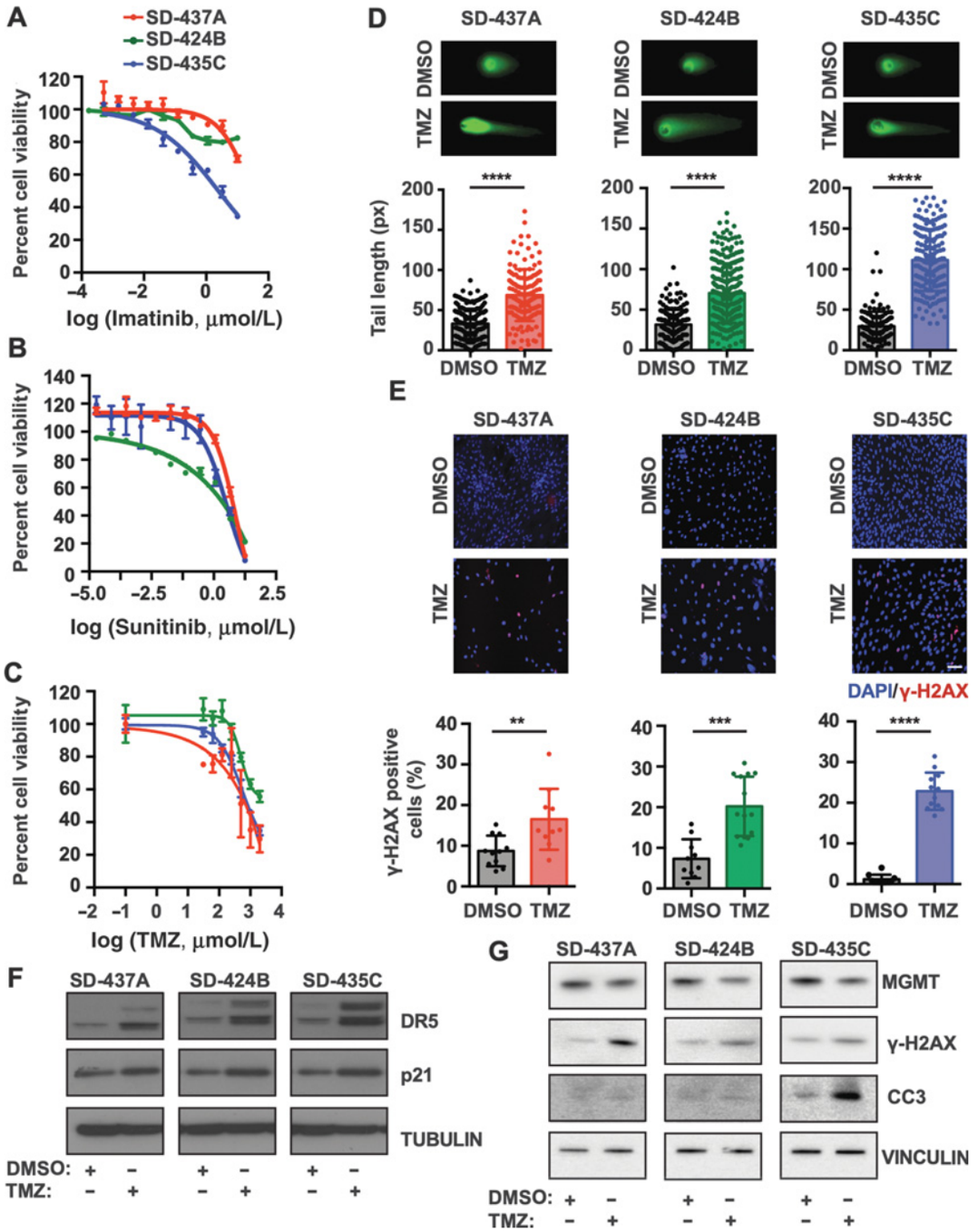

Figure 4.

Temozolomide reduces cell viability of m*SDH* GIST models by induction of DNA DSBs and impairing DNA repair. Cell viability of m*SDH* GIST models determined by CellTiter-Glo viability assay after treatment by imatinib (**A**), sunitinib (**B**), and temozolomide (**C**). Viability was measured after 3 days of treatment for imatinib and sunitinib and on 7 days of temozolomide treatment. Data are presented as mean ± SD. **D,** Representative images of a neutral comet assay for m*SDH* GIST models treated with either DMSO or 500 μmol/L temozolomide for 72 hours. Comet tail lengths were measured ($n = 100+$ cells per group) and plotted. **E,** Representative immunofluorescence images of m*SDH* GIST models treated with DMSO or temozolomide (500 μmol/L) and stained for γ-H2AX$^+$ nuclei. Quantification of γ-H2AX$^+$ cells in m*SDH* GIST models treated with DMSO or temozolomide for 72 hours. For each GIST model, γ-H2AX$^+$ nuclei were quantified and shown as % of total nuclei. Mann–Whitney *t* test was performed for statistical analysis with **, $P < 0.01$; ***, $P < 0.001$, ****, $P < 0.0001$. **F,** Immunoblots of m*SDH* GIST models treated with DMSO or temozolomide (500 μmol/L) for 3 days and probed for indicated proteins. **G,** Immunoblots of m*SDH* GIST models treated with DMSO or temozolomide (500 μmol/L) for 7 days and probed for indicated proteins. CC3 denotes cleaved caspase 3.

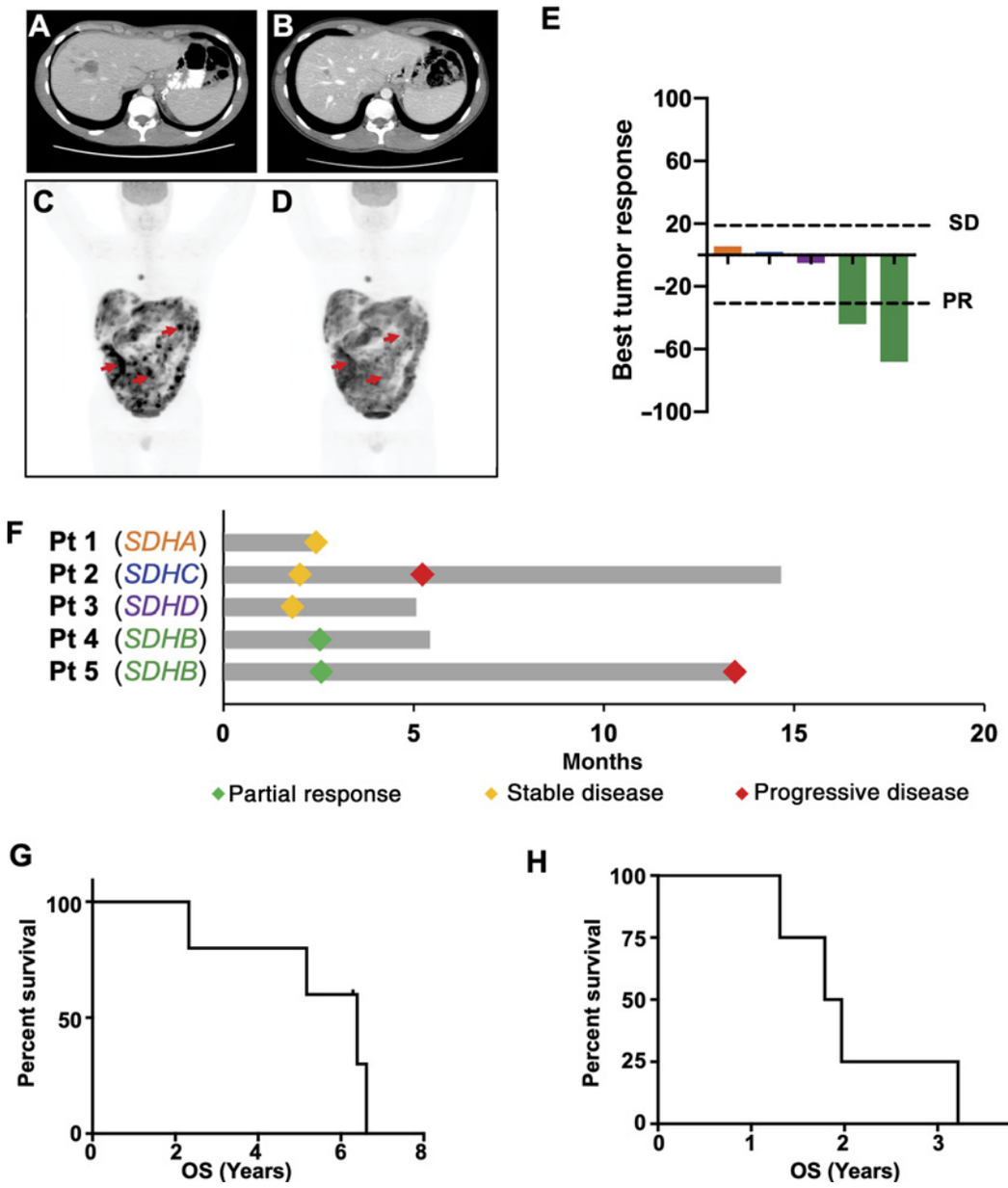

Figure 5.

Human *SDH*-mutant GISTs are sensitive to temozolomide. **A–D,** CT scan of a 22-year old male (Patient 5) with *SDHB*-mutant GIST before (**A**) and after 9 months of temozolomide (**B**), and PET scan of a 31-year old male (Patient 4) with *SDHB*-mutant GIST before (**C**) and after two cycles of temozolomide (**D**). Red arrows indicate representative examples of tumor responses to temozolomide. **E,** Waterfall plot demonstrating best tumor responses in 5 *SDH*-mutant GIST patients treated with temozolomide. **F,** Swimmer plot demonstrating PR, stable disease, and progressive disease in the same patients with *SDH*-mutant GIST treated with temozolomide depicted in **E**. Kaplan–Meier survival curves for patients with SDH-deficient GIST treated with temozolomide. Overall survival (OS) from date of diagnosis (**G**) and OS from start of temozolomide treatment (**H**).

screening. To date, genetic depletion in established human non-GIST cell lines, murine or hamster cells has been employed to mimic the loss of SDH complex in tumors (10–18). These studies were informative regarding major processes being affected by succinate accumulation and SDH loss; however, are not appropriate models for studying SDH-deficient GIST biology or personalized drug screening as they do not recapitulate the physiologic levels of SDH loss and fail to integrate the tissue specificity and patient-specific genetic-epigenetic aberrations along with SDH loss. To date, two PDX models have been established for SDH-deficient GIST. In one of these models, the tumor also had *KRAS* mutation, which is very uncommon in SDH-deficient GIST (19). Flavahan and colleagues established another PDX model from an SDH-deficient patient that was demonstrated to be sensitive to FGFR inhibitors. A combination of FGFR and KIT inhibition was found to be even more potent against these tumors (20). However, clonal selection in a murine environment, as well as cost and time required to establish

PDX models limits personalized drug screening. Here, we describe for the first time the establishment, propagation and characterization of unique patient-derived *SDH A/B/C*-mutant GIST cell models and this pipeline can be utilized for personalized drug screening for clinical application.

In this study, we describe a novel pipeline to establish patient-derived SDH GIST models that can be directly utilized for identifying new therapeutic agents and personalized drug screening of these patients. Our patient-derived m*SDH* GIST models established in this study express classical GIST markers (i.e., KIT and DOG-1), have low to undetectable levels of SDHB protein, and retain the molecular profiles of their corresponding patient tumors. In addition, they have the predicted metabolic signature of *SDH* enzyme complex loss, including elevated succinate, increased reductive carboxylation and diminished mitochondrial function, thus making them sensitive to metabolic inhibitors. We further demonstrate that these cells have elevated levels of HIF1α and HIF2α and activation of downstream targets relative to WT-*SDH* GIST cells under normoxia. Collectively, our models reliably recapitulate the metabolic, transcriptional, and proteomic profiles of parent tumors and also validate the characteristics of SDH-complex loss (**Fig. 6**).

Furthermore, the characteristic TKI resistance of these tumors is also recapitulated by these models *in vitro*. An important and novel finding in this study is that metabolic defects present in m*SDH* GIST models render them sensitive to the DNA alkylating agent temozolomide, which induces DNA damage and apoptotic cell death. Hadoux and colleagues, in a study with m*SDHB* PGL and PCC, observed 50% of *SDHB*-mutant patients had PRs and 40% had stable disease with temozolomide treatment, whereas no *SDHB* wildtype patients had PRs and 40% had progressive disease (53). However, the drug sensitivity varies in different tissues and hence we wanted to test the efficacy of temozolomide in GIST as they have different cells of origin than PCC and PGL. To date, two studies have evaluated the efficacy of temozolomide in patients with GIST but without reported genomic data (54, 55). The objective response rates were 0% in both studies of 18 patients each, suggesting that temozolomide is ineffective in unselected patients with GIST. The observed *in vitro* effects of temozolomide in our m*SDH* GIST models have clinical and translational relevance, as SDH-deficient GISTs differ from *KIT*-mutant tumors not only in terms of genetics, but also in terms of clinical features, patient outcomes, and TKI responsiveness. In the current study, we now report that temozolomide has promising activity in a cohort of patients with SDH-deficient GIST with disease progressing on prior therapies, resulting in either PRs or stabilization of disease in all patients. This represents a major advance for patients and the field.

In conclusion, we have developed and characterized novel patient-derived m*SDH* GIST models that recapitulate the cellular and molecular biology of m*SDH* GIST and are sensitive to temozolomide (**Fig. 6**).

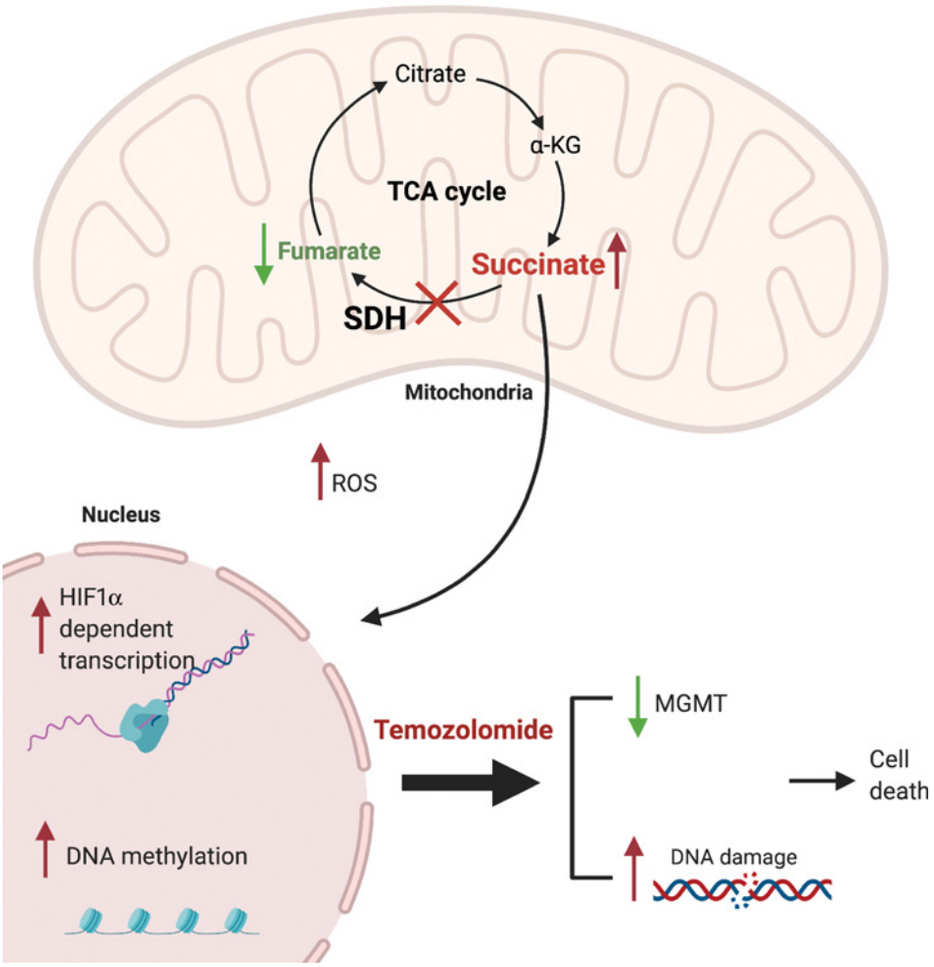

Figure 6.
Characteristics of m*SDH* models and proposed mechanism of action of temozolomide. Schematic representation highlighting metabolic and transcriptional characteristics of SDH-deficient parental tumors recapitulated by our patient-derived m*SDH* GIST models. Mechanism of action for temozolomide proposed is also depicted. Temozolomide induces DNA damage, reduces the MGMT levels, and leads to apoptosis. Created with BioRender.com.

Moreover, analysis of patients with SDH-deficient GIST treated with temozolomide indicates that this is a promising treatment for these patients and demonstrates that our m*SDH* GIST models are amenable for high-throughput drug testing. Based upon this early efficacy signal, we have opened a multi-institutional phase II study of single-agent temozolomide (NCT03556384) in patients with SDH-deficient GIST.

Authors' Disclosures

A.M. Burgoyne reports personal fees from Deciphera, Genentech, and Exelixis outside the submitted work. S.J. Advani reports grants from NIH during the conduct of the study as well as grants from NIH outside the submitted work. M.C. Heinrich reports personal fees from Novartis, Deciphera, and Blueprint Medicines, and grants from Department of Veterans Affairs during the conduct of the study. R. Kurzrock reports grants, personal fees, and other support from Boehringer Ingelheim, Debiopharm, Foundation Medicine, Genentech, Grifols, Guardant, Incyte, Konica Minolta, Medimmune, Merck Serono, Omniseq, Pfizer, Sequenom, Takeda, and TopAlliance; consultant and/or speaker fees and/or advisory board for Actuate Therapeutics, AstraZeneca, Bicara Therapeutics, Inc., Biological Dynamics, Eisai, EOM Pharmaceuticals, Iylon, Merck, NeoGenomics, Neomed, Pfizer, Prosperdtx, Regeneron, Roche, TD2/Volastra, Turning Point Therapeutics, and X-Biotech; has an equity interest in CureMatch Inc. and IDbyDNA; serves on the Board of CureMatch and CureMetrix; and is a co-founder of CureMatch outside the submitted work. O. Harismendy reports shares in Novartis and Sanofi. C. Metallo reports grants from NIH and FDA during the conduct of the study as well as personal fees from Rheos Medicines and Nimbus Therapeutics outside the submitted work. J.K. Sicklick reports other support from Amgen Pharmaceuticals and Foundation Medicine during the conduct of the study as well as personal fees from Deciphera, Foundation Medicine, Hoffman-La Roche, Merck, MJH Life Sciences, and QED Therapeutics, and other support from Personalis outside the submitted work. No disclosures were reported by the other authors.

Authors' Contributions

M. Yebra: Conceptualization, investigation, visualization, methodology, writing–original draft, writing–review and editing. **S. Bhargava:** Formal analysis, investigation, visualization, writing–original draft, writing–review and editing. **A. Kumar:** Formal analysis, investigation, writing–original draft, writing–review and editing. **A.M. Burgoyne:** Data curation, formal analysis, funding acquisition, investigation, visualization, writing–review and editing. **C.-M. Tang:** Formal analysis, investigation, writing–review and editing. **H. Yoon:** Formal analysis, investigation, writing–review and editing. **S. Banerjee:** Formal analysis, investigation, writing–review and editing. **J. Aguilera:** Formal analysis, investigation, writing–review and editing. **T. Cordes:** Formal analysis, investigation, methodology, writing–original draft, writing–review and editing. **V. Sheth:** Formal analysis, visualization, writing–review and editing. **S. Noh:** Investigation, writing–review and editing. **R. Ustoy:** Investigation, writing–review and editing. **S. Li:** Writing–review and editing. **S.J. Advani:** Investigation, methodology, writing–review and editing. **C.L. Corless:** Investigation, writing–review and editing. **M.C. Heinrich:** Investigation, writing–review and editing. **R. Kurzrock:** Investigation, writing–review and editing. **S.M. Lippman:** Investigation, writing–review and editing. **P.T. Fanta:** Conceptualization, resources, investigation, writing–review and editing. **O. Harismendy:** Data curation, software, formal analysis, supervision, investigation, writing–review and editing. **C. Metallo:** Conceptualization, resources, supervision, funding acquisition, methodology, writing–original draft, project administration, writing–review and editing. **J.K. Sicklick:** Conceptualization, resources, supervision, funding acquisition, methodology, writing–original draft, project administration, writing–review and editing.

Acknowledgments

This work was supported by FDA (R01 FD006334, J.K. Sicklick, C. Metallo), NIH grant R01 CA226803 (J.K. Sicklick), NIH grant R37 CA215081 (S.J. Advani), NIH grants R01 CA188652 and R01 CA234245 (C. Metallo.), GIST Research Fund (J.K. Sicklick), SDH Research Fund (J.K. Sicklick), Pedal the Cause (J.K. Sicklick, A.M. Burgoyne), Kristen Ann Carr Fund (J.K. Sicklick), and NSF CAREER Award (#1454425). It was also supported in part by Biorepository and Tissue Technology Shared Resource and NIH grant P30CA023100 (S.M. Lippman). We thank the Cancer Center Microscopy core (supported by NCI P30CA023100) for providing microscopes and imaging systems. We thank K. Jepsen at the University of California San Diego IGM Genomics Center (supported by NIH grant P30CA023100) for generation and sequencing of mRNA libraries. We also thank D. Jaquish and R. French for helpful discussions and collaboration. Finally, and most importantly, we thank the Melikian Hatounian family, the MacLea family, and SDH Research Advocates for their inspiration and support.

Dedication

This work is dedicated to the memory of Merak Melikian Hatounian, who inspired this work and bravely fought his disease with the utmost courage, dignity, and determination.

The costs of publication of this article were defrayed in part by the payment of page charges. This article must therefore be hereby marked *advertisement* in accordance with 18 U.S.C. Section 1734 solely to indicate this fact.

Received June 8, 2021; revised August 19, 2021; accepted August 19, 2021; published first August 23, 2021.

References

1. Neppala P, Banerjee S, Fanta PT, Yerba M, Porras KA, Burgoyne AM, et al. Current management of succinate dehydrogenase-deficient gastrointestinal stromal tumors. Cancer Metastasis Rev 2019;38:525–35.
2. Gebreyohannes YK, Wozniak A, Zhai ME, Wellens J, Cornillie J, Vanleeuw U, et al. Robust activity of avapritinib, potent and highly selective inhibitor of mutated KIT, in patient-derived xenograft models of gastrointestinal stromal tumors. Clin Cancer Res 2019;25:609–18.
3. Carney JA, Stratakis CA. Familial paraganglioma and gastric stromal sarcoma: a new syndrome distinct from the Carney triad. Am J Med Genet 2002;108:132–9.
4. Pasini B, McWhinney SR, Bei T, Matyakhina L, Stergiopoulos S, Muchow M, et al. Clinical and molecular genetics of patients with the Carney-Stratakis syndrome and germline mutations of the genes coding for the succinate dehydrogenase subunits SDHB, SDHC, and SDHD. Eur J Hum Genet 2008; 16:79–88.
5. Killian JK, Kim SY, Miettinen M, Smith C, Merino M, Tsokos M, et al. Succinate dehydrogenase mutation underlies global epigenomic divergence in gastrointestinal stromal tumor. Cancer Discov 2013;3:648–57.
6. Rubin BP, Antonescu CR, Scott-Browne JP, Comstock ML, Gu Y, Tanas MR, et al. A knock-in mouse model of gastrointestinal stromal tumor harboring kit K641E. Cancer Res 2005;65:6631–9.
7. Taguchi T, Sonobe H, Toyonaga S, Yamasaki I, Shuin T, Takano A, et al. Conventional and molecular cytogenetic characterization of a new human cell line, GIST-T1, established from gastrointestinal stromal tumor. Lab Invest 2002; 82:663–5.
8. Na YS, Ryu MH, Park YS, Lee CW, Lee JK, Park Y, et al. Establishment of patient-derived xenografts from patients with gastrointestinal stromal tumors: analysis of clinicopathological characteristics related to engraftment success. Sci Rep 2020;10:7996.
9. Sommer G, Agosti V, Ehlers I, Rossi F, Corbacioglu S, Farkas J, et al. Gastrointestinal stromal tumors in a mouse model by targeted mutation of the Kit receptor tyrosine kinase. Proc Natl Acad Sci U S A 2003;100:6706–11.
10. Aspuria PP, Lunt SY, Varemo L, Vergnes L, Gozo M, Beach JA, et al. Succinate dehydrogenase inhibition leads to epithelial-mesenchymal transition and reprogrammed carbon metabolism. Cancer Metab 2014;2:21.
11. Selak MA, Armour SM, MacKenzie ED, Boulahbel H, Watson DG, Mansfield KD, et al. Succinate links TCA cycle dysfunction to oncogenesis by inhibiting HIF-alpha prolyl hydroxylase. Cancer Cell 2005;7:77–85.
12. Guzy RD, Sharma B, Bell E, Chandel NS, Schumacker PT. Loss of the SdhB, but Not the SdhA, subunit of complex II triggers reactive oxygen species-dependent hypoxia-inducible factor activation and tumorigenesis. Mol Cell Biol 2008;28: 718–31.
13. Morin A, Goncalves J, Moog S, Castro-Vega LJ, Job S, Buffet A, et al. TET-mediated hypermethylation primes SDH-deficient cells for HIF2alpha-driven mesenchymal transition. Cell Rep 2020;30:4551–66.

14. Kluckova K, Thakker A, Vettore L, Escribano-Gonzalez C, Hindshaw RL, Tearle JLE, et al. Succinate dehydrogenase deficiency in a chromaffin cell model retains metabolic fitness through the maintenance of mitochondrial NADH oxidoreductase function. FASEB J 2020;34:303–15.
15. Xiao M, Yang H, Xu W, Ma S, Lin H, Zhu H, et al. Inhibition of alpha-KG-dependent histone and DNA demethylases by fumarate and succinate that are accumulated in mutations of FH and SDH tumor suppressors. Genes Dev 2012; 26:1326–38.
16. Loriot C, Domingues M, Berger A, Menara M, Ruel M, Morin A, et al. Deciphering the molecular basis of invasiveness in Sdhb-deficient cells. Oncotarget 2015; 6:32955–65.
17. Wang H, Chen Y, Wu G. SDHB deficiency promotes TGFbeta-mediated invasion and metastasis of colorectal cancer through transcriptional repression complex SNAIL1-SMAD3/4. Transl Oncol 2016;9:512–20.
18. Soderberg KL, Ditta GS, Scheffler IE. Mammalian cells with defective mitochondrial functions: a Chinese hamster mutant cell line lacking succinate dehydrogenase activity. Cell 1977;10:697–702.
19. Powers JF, Cochran B, Baleja JD, Sikes HD, Zhang X, Lomakin I, et al. A unique model for SDH-deficient GIST: an endocrine-related cancer. Endocr Relat Cancer 2018;25:943–54.
20. Flavahan WA, Drier Y, Johnstone SE, Hemming ML, Tarjan DR, Hegazi E, et al. Altered chromosomal topology drives oncogenic programs in SDH-deficient GISTs. Nature 2019;575:229–33.
21. Beattie GM, Cirulli V, Lopez AD, Hayek A. *Ex vivo* expansion of human pancreatic endocrine cells. J Clin Endocrinol Metab 1997;82:1852–6.
22. Livak KJ, Schmittgen TD. Analysis of relative gene expression data using real-time quantitative PCR and the 2(-Delta Delta C(T)) Method. Methods 2001;25: 402–8.
23. Cosset E, Ilmjarv S, Dutoit V, Elliott K, von Schalscha T, Camargo MF, et al. Glut3 addiction is a druggable vulnerability for a molecularly defined subpopulation of glioblastoma. Cancer Cell 2017;32:856–68.e5.
24. Wang X, Spandidos A, Wang H, Seed B. PrimerBank: a PCR primer database for quantitative gene expression analysis, 2012 update. Nucleic Acids Res 2012;40: D1144–9.
25. Untergasser A, Cutcutache I, Koressaar T, Ye J, Faircloth BC, Remm M, et al. Primer3–new capabilities and interfaces. Nucleic Acids Res 2012;40:e115.
26. Advani SJ, Camargo MF, Seguin L, Mielgo A, Anand S, Hicks AM, et al. Kinase-independent role for CRAF-driving tumour radioresistance via CHK2. Nat Commun 2015;6:8154.
27. Cordes T, Metallo CM. Quantifying intermediary metabolism and lipogenesis in cultured mammalian cells using stable isotope tracing and mass spectrometry. Methods Mol Biol 2019;1978:219–41.
28. Divakaruni AS, Rogers GW, Murphy AN. Measuring mitochondrial function in permeabilized cells using the seahorse XF analyzer or a clark-type oxygen electrode. Curr Protoc Toxicol 2014;60:25.2.1–16.
29. Eisenhauer EA, Therasse P, Bogaerts J, Schwartz LH, Sargent D, Ford R, et al. New response evaluation criteria in solid tumours: revised RECIST guideline (version 1.1). Eur J Cancer 2009;45:228–47.
30. Wahl RL, Jacene H, Kasamon Y, Lodge MA. From RECIST to PERCIST: evolving considerations for PET response criteria in solid tumors. J Nucl Med 2009;50: 122S–50S.
31. Saxena NK, Sharma D, Ding X, Lin S, Marra F, Merlin D, et al. Concomitant activation of the JAK/STAT, PI3K/AKT, and ERK signaling is involved in leptin-mediated promotion of invasion and migration of hepatocellular carcinoma cells. Cancer Res 2007;67:2497–507.
32. Dobin A, Davis CA, Schlesinger F, Drenkow J, Zaleski C, Jha S, et al. STAR: ultrafast universal RNA-seq aligner. Bioinformatics 2013;29:15–21.
33. Love MI, Huber W, Anders S. Moderated estimation of fold change and dispersion for RNA-seq data with DESeq2. Genome Biol 2014;15:550.
34. Vlodavsky I, Lui GM, Gospodarowicz D. Morphological appearance, growth behavior and migratory activity of human tumor cells maintained on extracellular matrix versus plastic. Cell 1980;19:607–16.
35. Tuveson DA, Willis NA, Jacks T, Griffin JD, Singer S, Fletcher CD, et al. STI571 inactivation of the gastrointestinal stromal tumor c-KIT oncoprotein: biological and clinical implications. Oncogene 2001;20:5054–8.
36. Lussey-Lepoutre C, Hollinshead KE, Ludwig C, Menara M, Morin A, Castro-Vega LJ, et al. Loss of succinate dehydrogenase activity results in dependency on pyruvate carboxylation for cellular anabolism. Nat Commun 2015; 6:8784.
37. Cardaci S, Zheng L, MacKay G, van den Broek NJ, MacKenzie ED, Nixon C, et al. Pyruvate carboxylation enables growth of SDH-deficient cells by supporting aspartate biosynthesis. Nat Cell Biol 2015;17:1317–26.
38. Muhlenberg T, Grunewald S, Treckmann J, Podleska L, Schuler M, Fletcher JA, et al. Inhibition of KIT-glycosylation by 2-deoxyglucose abrogates KIT-signaling and combination with ABT-263 synergistically induces apoptosis in gastrointestinal stromal tumor. PLoS One 2015;10:e0120531.
39. Jacob F, Salinas RD, Zhang DY, Nguyen PTT, Schnoll JG, Wong SZH, et al. A patient-derived glioblastoma organoid model and Biobank recapitulates inter- and intra-tumoral heterogeneity. Cell 2020;180:188–204.e22.
40. Cervera AM, Apostolova N, Crespo FL, Mata M, McCreath KJ. Cells silenced for SDHB expression display characteristic features of the tumor phenotype. Cancer Res 2008;68:4058–67.
41. Yang M, Pollard PJ. Succinate: a new epigenetic hacker. Cancer Cell 2013;23: 709–11.
42. Lopez-Jimenez E, Gomez-Lopez G, Leandro-Garcia LJ, Munoz I, Schiavi F, Montero-Conde C, et al. Research resource: Transcriptional profiling reveals different pseudohypoxic signatures in SDHB and VHL-related pheochromocytomas. Mol Endocrinol 2010;24:2382–91.
43. Yang L, Forker L, Irlam JJ, Pillay N, Choudhury A, West CML. Validation of a hypoxia related gene signature in multiple soft tissue sarcoma cohorts. Oncotarget 2018;9:3946–55.
44. Tena I, Gupta G, Tajahuerce M, Benavent M, Cifrian M, Falcon A, et al. Successful second-line metronomic temozolomide in metastatic paraganglioma: case reports and review of the literature. Clin Med Insights Oncol 2018;12: 11795549.
45. Bravo EL, Kalmadi SR, Gill I. Clinical utility of temozolomide in the treatment of malignant paraganglioma: a preliminary report. Horm Metab Res 2009;41:703–6.
46. Lee SY. Temozolomide resistance in glioblastoma multiforme. Genes Dis 2016;3: 198–210.
47. Cui B, Johnson SP, Bullock N, Ali-Osman F, Bigner DD, Friedman HS. Decoupling of DNA damage response signaling from DNA damages underlies temozolomide resistance in glioblastoma cells. J Biomed Res 2010;24: 424–35.
48. Fu D, Calvo JA, Samson LD. Balancing repair and tolerance of DNA damage caused by alkylating agents. Nat Rev Cancer 2012;12:104–20.
49. Tentori L, Graziani G. Recent approaches to improve the antitumor efficacy of temozolomide. Curr Med Chem 2009;16:245–57.
50. Natsume A, Ishii D, Wakabayashi T, Tsuno T, Hatano H, Mizuno M, et al. IFN-beta down-regulates the expression of DNA repair gene MGMT and sensitizes resistant glioma cells to temozolomide. Cancer Res 2005; 65:7573–9.
51. Ryu CH, Yoon WS, Park KY, Kim SM, Lim JY, Woo JS, et al. Valproic acid downregulates the expression of MGMT and sensitizes temozolomide-resistant glioma cells. J Biomed Biotechnol 2012;2012:987495.
52. Kohsaka S, Wang L, Yachi K, Mahabir R, Narita T, Itoh T, et al. STAT3 inhibition overcomes temozolomide resistance in glioblastoma by downregulating MGMT expression. Mol Cancer Ther 2012;11:1289–99.
53. Hadoux J, Favier J, Scoazec JY, Leboulleux S, Al Ghuzlan A, Caramella C, et al. SDHB mutations are associated with response to temozolomide in patients with metastatic pheochromocytoma or paraganglioma. Int J Cancer 2014;135:2711–20.
54. Trent JC, Beach J, Burgess MA, Papadopolous N, Chen LL, Benjamin RS, et al. A two-arm phase II study of temozolomide in patients with advanced gastrointestinal stromal tumors and other soft tissue sarcomas. Cancer 2003; 98:2693–9.
55. Garcia del Muro X, Lopez-Pousa A, Martin J, Buesa JM, Martinez-Trufero J, Casado A, et al. A phase II trial of temozolomide as a 6-week, continuous, oral schedule in patients with advanced soft tissue sarcoma: a study by the Spanish Group for Research on Sarcomas. Cancer 2005;104:1706–12.